Acta Cryst. (1995). D**51**, 368–379

Structure of the Photochemical Reaction Centre of a Spheroidene-Containing Purple Bacterium, *Rhodobacter sphaeroides* Y, at 3 Å Resolution

BY BERNADETTE ARNOUX,* JEAN-FRANÇOIS GAUCHER AND ARNAUD DUCRUIX

Laboratoire de Biologie Structurale, CNRS, 91198 Gif-sur-Yvette, France

AND FRANÇOISE REISS-HUSSON

Centre de Génétique Moléculaire, CNRS, 91198 Gif-sur-Yvette, France

(*Received* 11 *July* 1994; *accepted* 14 *November* 1994)

Abstract

The crystal structure of the photochemical reaction centre from *Rhodobacter sphaeroides* Y, a carotenoid-containing wild-type purple bacterium, has been determined at 3 Å resolution. This membrane complex consists of three subunits (281, 307 and 260 residues, respectively) and ten cofactors. It was crystallized in presence of β-D-octylglucoside. The crystals are orthorhombic with unit-cell dimensions, a = 143.7, b = 139.8, c = 78.7 Å, space group $P2_12_12_1$ with four molecules in the unit cell. Refinement of the structure by *X-PLOR* and manual reconstructions yielded an R value of 22.1% for 19 630 reflections between 7 and 3 Å. The secondary structure is highly homologous to those determined for *Rhodopseudomonas viridis* (Protein Data Bank entry 1PRC) and *Rhodobacter sphaeroides* R26 (Protein Data Bank entry 4RCR) reaction centres. In the latter two structures one Fe^{2+} ion located between the two quinones is coordinated by four histidines and one glutamic acid. In the *Rhodobacter sphaeroides* Y structure, Mn^{2+} occupies the same position with identical ligands and geometry. The carotenoid conformation which is a non-planar 15-15′-*cis* spheroidene molecule in our structure differs from the 13-14-*cis* 2,4-dihydroneusporene in the *Rhodopseudomonas viridis* structure.

Introduction

Photochemical reaction centres (RC's) of photosynthetic organisms are membrane-bound pigment–protein complexes which perform the initial step of energy conversion, a transmembrane light-induced charge separation. In purple bacteria such as *Rhodobacter* (*Rb.*) *sphaeroides*, the RC consists of three polypeptides, *L* (281 amino acids), *M* (307 amino acids) and *H* (260 amino acids), and several pigments and cofactor molecules associated with *L* and *M*: four bacteriochlorophylls (Bchl's), two bacteriopheophytins (Bpheo's), one carotenoid, two quinones and one metal ion. In other bacterial species including *Rhodopseudomonas* (*Rps.*) *viridis*, the RC is tightly associated with a tetraheme cytochrome subunit. Light excitation of the RC generates a stable charge-separated state, in which a dimer of strongly coupled Bchl's becomes oxidized, and a quinone, Q_B, is reduced. This occurs after a series of fast electron-transfer reactions through successive intermediate electron carriers: a Bchl, a Bpheo and a quinone, Q_A.

A molecular description of these processes was achieved when the crystal structure of the RC of *Rps. viridis*, with its bound cytochrome subunit, was solved (Deisenhofer, Epp, Miki, Huber & Michel, 1985*a*,*b*). The structure of the RC of *Rb. sphaeroides* R26 (this strain is a carotenoidless mutant) was then described by two independent groups (Allen, Feher, Yeates, Komiya & Rees, 1988; Chang, El-Kabbani, Tiede, Norris & Schiffer, 1991; El-Kabbani, Chang, Tiede, Norris & Schiffer, 1991). It was highly homologous to *Rps. viridis* RC (except for the absence of the cytochrome unit). The dominant feature of these structures is the presence of 11 hydrophobic α-helices (which *in vivo* span the membrane), five in *L*, five in *M* and one in *H*. The helices in *L* and *M* are related by a pseudo-twofold symmetry axis. This axis, running through the Bchl dimer and the metal ion, also applies to the pigment assembly (except for the carotenoid molecule).

These crystallographic studies were extended to RC's from several wild-type strains of *Rb. sphaeroides*: strains Y (Ducruix & Reiss-Husson, 1987; Arnoux *et al.*, 1989); 2.4.1 (Yeates *et al.*, 1988) and ATCC 17023 (Buchanan, Fritzch, Ermler & Michel, 1993). RC's from these strains differ from the R26 RC by the presence of spheroidene, a carotenoid which does not transfer electrons but protects Bchl's from photodestruction (Cogdell & Frank, 1987). A distinctive property of the Y strain is the presence of Mn^{2+} as the metal ion which interacts with the quinones instead of Fe^{2+} as in the other RC's; this Mn^{2+}, which has been characterized by its EPR properties in detergent solutions of the RC (Rutherford, Agalidis & Reiss-Husson, 1985), is still present in the crystals (Ducruix & Reiss-Husson, 1987).

* To whom correspondence should be addressed.

In this report, we describe the structure of Y RC refined at 3 Å resolution and compare it with RC structures refined already (Deisenhofer, Epp, Miki, Huber & Michel, 1985*a*,*b*; Michel, Epp & Deisenhofer, 1986; Deisenhofer & Michel, 1989; Komiya, Yeates, Rees, Allen & Feher, 1988). We focus mainly on the protein subunits, their secondary structures and their interactions which determine the overall architecture and cohesion of the complex. A detailed description of the pigments, cofactors and of the mode of binding of these molecules to neighbouring residues, will be published elsewhere (Arnoux, Ducruix & Reiss-Husson, 1995).

Material and methods

Crystal and diffraction data

RC from photosynthetically grown *Rb. sphaeroides* Y cells was isolated and purified as already described using lauryl-dimethylamine oxide (Fluka) as detergent (Ducruix, Arnoux & Reiss-Husson, 1988). In the final step this detergent was exchanged for β-D-octylglucoside (Bachem) by chromatography on a DEAE–Sepharose column equilibrated with 15 m*M* Tris–HCl buffer, pH 8.0, containing 1 m*M* EDTA and 8 mg ml^{-1} β-D-octylglucoside. After adsorption and extensive washing, the RC was eluted by 1 *M* NaCl in the same buffer and desalted on a Sephadex G25 column. Final concentration was obtained by ultrafiltration on Centricon 30 cells.

The nucleotide sequence of the region which contains the *pufL*, *pufM* and *pufH* genes was determined by the chain-termination method of Sanger using base-denatured double-stranded plasmids as templates (EMBL accession numbers: X63378, X63404, X63405). It only shows one sequence difference at position *M*140 (Leu to Met) as compared to the 241-type strain (Williams, Steiner & Feher, 1986).

Crystallization was carried out by microdialysis (Ducruix, Arnoux & Reiss-Husson, 1988) at 291 K, with equilibrium concentrations of 2 mg ml^{-1} protein, 12.5–14.5% PEG 4000, 0.22 *M* NaCl, 8 mg ml^{-1} β-D-octylglucoside, in a 15 m*M* Tris–HCl buffer, pH 8.0, containing 1 m*M* EDTA and 0.1% sodium azide. PEG was purified before use (Ray & Puvathingal, 1985). The microdialysis was performed in the dark and in closed vials which were initially flushed with argon; this was found to prevent the slow oxidation of the RC, as observed by spectrophotometry of single crystals (Reiss-Husson & Mäntele, 1988).

Orthorhombic crystals grew as long rods (maximum size 0.4 × 0.3 × 1.5 mm) with a diamond-shaped cross-section with elongation along the *a* axis. Highly diffracting crystals (3.0 Å) were difficult to obtain. Quite often hollow crystals or excessive nucleation led to useless batches. Crystals belong to the orthorhombic system, space group $P2_12_12_1$, with cell dimensions a = 143.7, b = 139.8, c = 78.65 Å and one complex per asymmetric unit. Because of the rapid decay of crystals during irradiation, X-ray intensity data were measured on several crystals, with average size 0.4 × 0.4 × 0.8 mm at the D43 beamline (λ = 1.38 Å) using the synchrotron radiation source at LURE (Orsay). A full set of data was collected on a dozen of crystals in 1.2 to 2° oscillation steps over a φ range of 93° to a resolution of

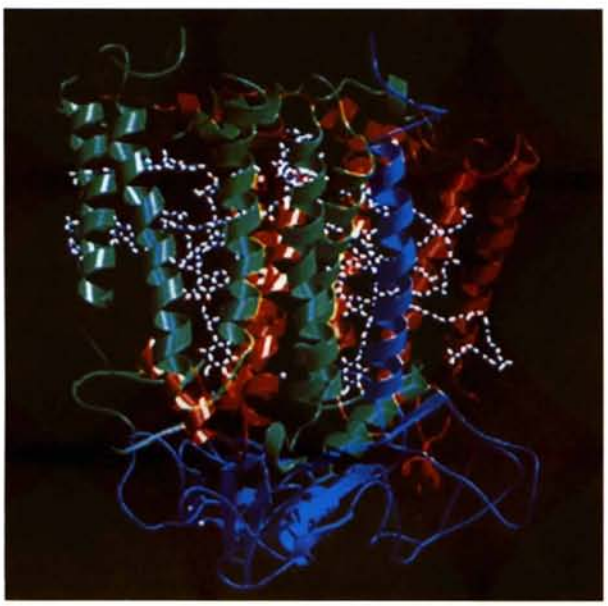

(*a*)

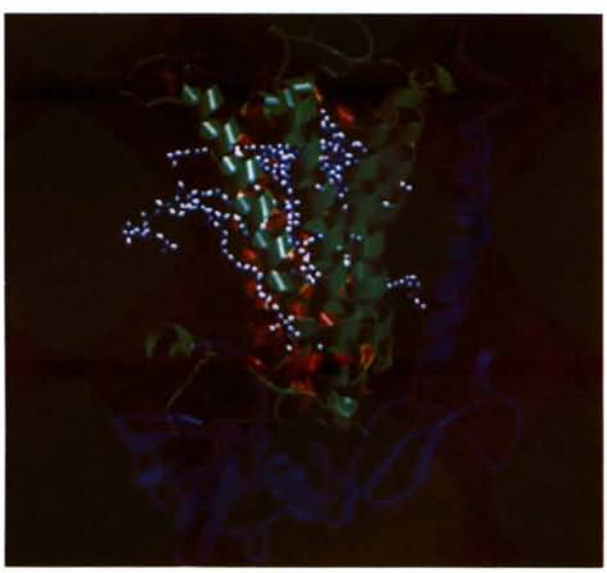

(*b*)

Fig. 1. Schematic drawings of the RC from *Rb. sphaeroides* Y. The α-helices are drawn as wound ribbons, the β-strands as arrows, the pigments and cofactors as ball-and-stick diagrams. The *L* subunit is coloured in red, *M* in green, *H* in blue. The pseudo-twofold axis is vertical and in the figure plane. Views (*a*) and (*b*) differ by a 90° rotation around this axis. Prepared with *MOLSCRIPT* (Krauiis, 1991).

3.0 Å; the crystal-to-film distance was 90 mm. The X-ray diffraction pattern was anisotropic with lower resolution along the crystallographic *b* axis. Two impacts were generally used on each crystal after a rotation of 10° to minimize the effects of radiation damage. The data were processed using the *DENZO* package (Otwinowski, 1993); *ROTAVATA* and *AGROVATA* from the *CCP*4 package (Collaborative Computational Project, Number 4, 1994) were used to scale and merge the data. R_{sym} between 50 and 3 Å resolution is 13.8% for 24 200 reflections which correspond to 80% completeness.

Structure and refinement

When this work was in progress, two crystal structures of RC from *Rb. sphaeroides* R26 (a carotenoidless mutant) were under refinement. RC's from the R26 and the wild-type strains crystallize in the same space group with nearly isomorphous unit cells. We used the structure of R26 RC (Chang *et al.*, 1986) as a starting model for the refinement.

The first step was a rigid-body refinement. It was followed by one complete cycle of *X-PLOR* refinement applied to the three polypeptide chains and all the pigments except the quinones and the carotenoid. At the end of this first cycle a difference-Fourier map showed without ambiguity the location of spheroidene and both quinones.

During this first cycle of refinement, topology and parameter files used for pigments and cofactors were those kindly provided by H. Treutlein. The choice of these parameters is a matter of debate, as only a few crystal structures of pigments are determined with accuracy. Another set of parameter files, determined by Foloppe, Ferrand, Breton & Smith (1995) for their work on reaction-centre modelling became available to us and was used for another complete cycle of refinement at 3.5 Å resolution. Several cycles of manual rebuilding (Jones, 1978), simulated annealing and Powell minimization (*X-PLOR* 3.0, Brünger, Kuriyan & Karplus, 1987) were performed. As described below, electron density in the transmembrane region was always of better quality than in the surface regions. The crystallographic *R* factor at 3.5 Å was 24.5% for reflections with $F_o > 2\sigma$ with an overall *B* factor of 28 Å^2.

When *X-PLOR* Version 3.1 was released, a new set of force fields was distributed (Engh & Huber, 1991). A trial was carried out to modify the force-field files for pigment and cofactors in agreement with those for protein. A cycle of refinement was carried out at 3.5 Å resolution and continued by Powell minimization extending the resolution to 3.0 Å. As mentioned above, the diffraction pattern of these crystals was anisotropic with a *b* direction of poorer quality. So far, we have used *X-PLOR* to refine the general temperature factor in an anisotropic scheme.

Quality assessment of the final model

After individual temperature-factor refinement, a final *R* factor of 22.9% was obtained with 19 630 reflections between 7 and 3.0 Å, with reflections with $F_o/F_c > 2.5$ or $F_c/F_o > 2.5$ omitted, 4.5% of the whole data set (Brzozowski, Derewenda, Dodson, Dodson & Turkenburg, 1992). The refinement statistics and measurement of the quality of the geometry of the model are presented in Table 1. The mean *B* value for the 7136 atoms of the model is 34 Å^2. Most of the main-chain dihedral angles are within the allowed regions of the Ramachandran plot. All others correspond to residues in loop regions. The estimated error of atomic positions as derived from a Luzzati plot (Luzzati, 1952) is 0.4 Å.

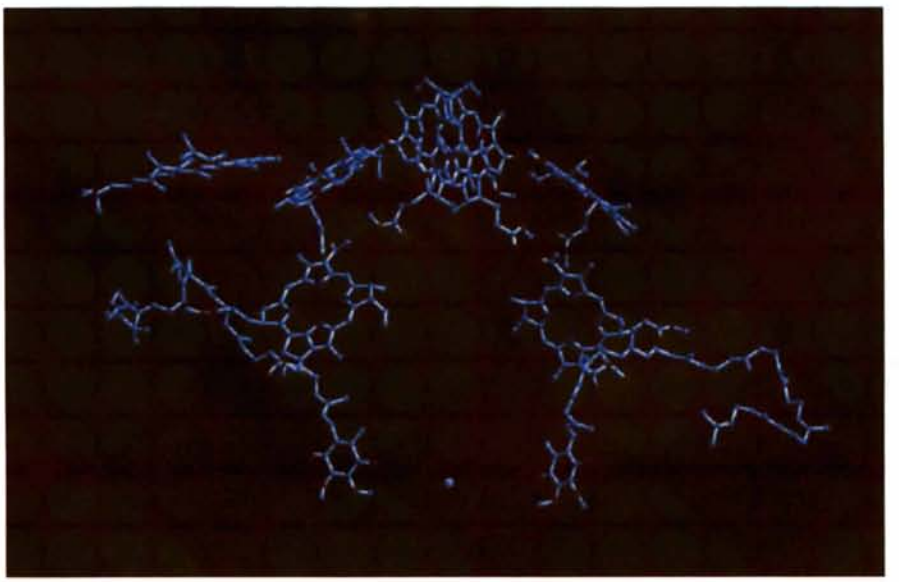

Fig. 2. Ball-and-stick model of the pigments and cofactors. Phytyl tails have been removed for clarity. The orientation is the same as in Fig. 1(*a*). From the Bchl's dimer (BC_{LP}/BC_{MP}) (top of the figure) the two branches of pigments consist of one monomeric Bchl (BC_{LA}/BC_{MA}), one Bpheo (BP_L/BP_M) and one ubiquinone (Q_A/Q_B). Spheroidene is located near BC_{MA}.

Table 1. *Refinement statistics*

R.m.s. deviation from ideality

Bonds (Å)	0.024
Angles (°)	2.5
Dihedral (°)	24.5
Improper (°)	2.1

Quality of the model

	L	*M*	*H*	Pigments
No. atoms	2181	2429	1973	553
B overall (Å^2)	31.9	33.8	39.0	31.2
Residue No. with tenuous density	60	98, 107, 120, 215, 221, 277, 300	31, 43, 52, 60, 126, 160, 210–212, 248, 260	Part of phytyl and isoprenoid chains*

* Arnoux, Ducruix & Reiss-Husson (1995).

The refined model represents 99% of the amino-acid chain of the RC molecule. The electron density around the *M*140 position can be modelled with a Met residue, in agreement with the sequence data which indicated it was the only residue modified in RC Y strain as compared to the RC 241-type strain (Arnoux *et al.*, 1990). There is no electron density for the eight C-terminal residues of the *L* chain and for the two C-terminal residues in the *H* chain. Regions with highest *B* value are: residues 57 and 58 of the *L* chain, residues 98, 110–111, 304–305 of the *M* chain, residues 1–5, 48–51, 80–82, 92–93 and 248–249 of the *H* chain. They correspond either to N or C termini, or to surface domains exposed to solvent. The electron density for the *H* chain is of poorer quality compared with the other two chains. The central Mg atoms of the four BCl's have a clearly defined electron density. The electron density for some parts of the phytyl chain of bacteriochlorophylls, bacteriopheophytins and Q_B tail is tenuous. At 3 Å resolution, localization of solvent or detergent would be ambiguous, except for tightly bounded molecules. No solvent or detergent molecules were positioned in this structure.

Definition of secondary structure

Accurate assignments of secondary structures of the subunits are crucial for a useful comparison between RC's. Three programs which automatically determine the location of helices and strands were used for this purpose, namely *DSSP* (Kabsch & Sander, 1983), *P-CURVE* (Sklenar, Etchebest & Lavery, 1989) and *DEFINE* (Richards & Kundrot, 1988). The distribution in length of helices and β-strands highlights the differences of each assignment algorithm. Because of these difficulties a consensus method, (Colloc'h, Etchebest, Thoreau, Henrissat & Mornon, 1993) in which each residue is assigned to secondary structure predicted by at least two of these three methods, was used.

Definition of hydrogen bonds and salt bridges

Hydrogen bonds were identified by applying the following criteria: a maximum distance between donor and acceptor atom of 3.5 Å and a minimum distance of 2.4 Å. For salt bridges, we used the same limits for distances between Asp or Glu and Lys or Arg residues.

Definition of solvent-accessible area

The program *AREA* from the *CCP*4 package was used to calculate solvent accessibility using Lee & Richards' algorithm (Lee & Richards, 1971). A probe sphere of 1.4 Å radius was used for the area calculations. Differences in accessibility were calculated between the solvent-accessible area of one isolated subunit and the solvent-accessible area of this subunit when associated with another one.

Structural results

General description and secondary structure

The overall structure of the wild-type RC from *Rb. sphaeroides* Y (Fig. 1) is very similar to that of *Rps. viridis* (Deisenhofer & Michel, 1989) and to those ob-

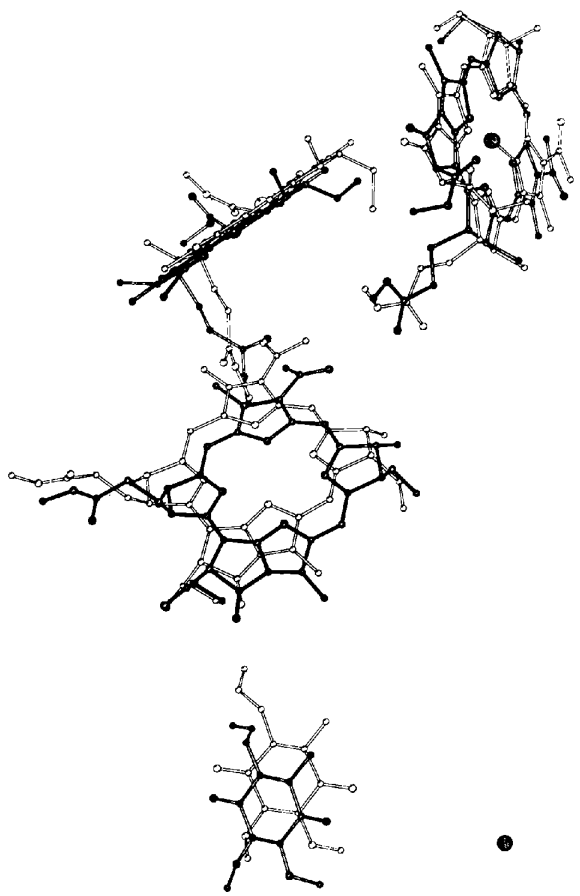

Fig. 3. Superposition of the two pigment branches (BC_{LP}, BC_{LA}, BP_L and Q_A drawn as white ball-and-stick diagrams; BC_{MP}, BC_{MA}, BP_M and Q_B as dark ones), when applying the pseudo-twofold symmetry to the former pigment branch. Phytyl and isoprenoid chains have been removed.

tained for the R26 mutant of *Rb. sphaeroides* (Allen, Feher, Yeates, Komiya & Rees, 1988; Chang, El-Kabbani, Tiede, Norris & Schiffer, 1991) and, therefore, will only be described briefly.

The pigment assembly is located within the *L* and *M* subunits, along two branches related by a local twofold symmetry axis (Fig. 2), which also relates the five hydrophobic α-helices of the *L* subunit, called *A*, *B*, *C*, *D* and *E*, to the corresponding ones of *M*. This axis is equidistant from the pyrrole N atoms of the Bchl's dimer, and passes through the Mn^{2+} ion. It applies to the porphyrin rings and to the quinone cycles, but not to the phytyl and isoprenoid tails of these molecules. Deviations from perfect local symmetry between pigment couples are increasing steadily from the dimer towards the quinones, as shown in Fig. 3. The spheroidene molecule is the only pigment molecule asymmetrically located on one of the pigment branches.

The overall height of the RC along the local symmetry axis is approximately 73 Å, providing about 30 Å for the hydrophobic core region (which has been shown to be covered in the crystal by detergent molecules, Roth, Arnoux, Ducruix & Reiss-Husson, 1991), 15 Å for the thickness of the polar periplasmic part (situated above the dimer), and 28 Å for that of the polar cytoplasmic part (on the opposite side). When looking at the RC complex at its thinnest width (Fig. 1*b*), the transmembrane bundle of helices adopt a '*V*' shape with a thickness of 35 Å near the periplasmic side and 26 Å near the cytoplasmic side. A 90° rotation around the pseudo-twofold axis (Fig. 1*a*) brings the RC into its largest width which is about 65 Å.

The secondary structure of wild-type RC was determined by a consensus method (see above) (Fig. 4). The hydrophobic α-helices *A* to *E* of *L* and *M* (Table 2), and the only one of *H*, with a mean length of 25 Å are

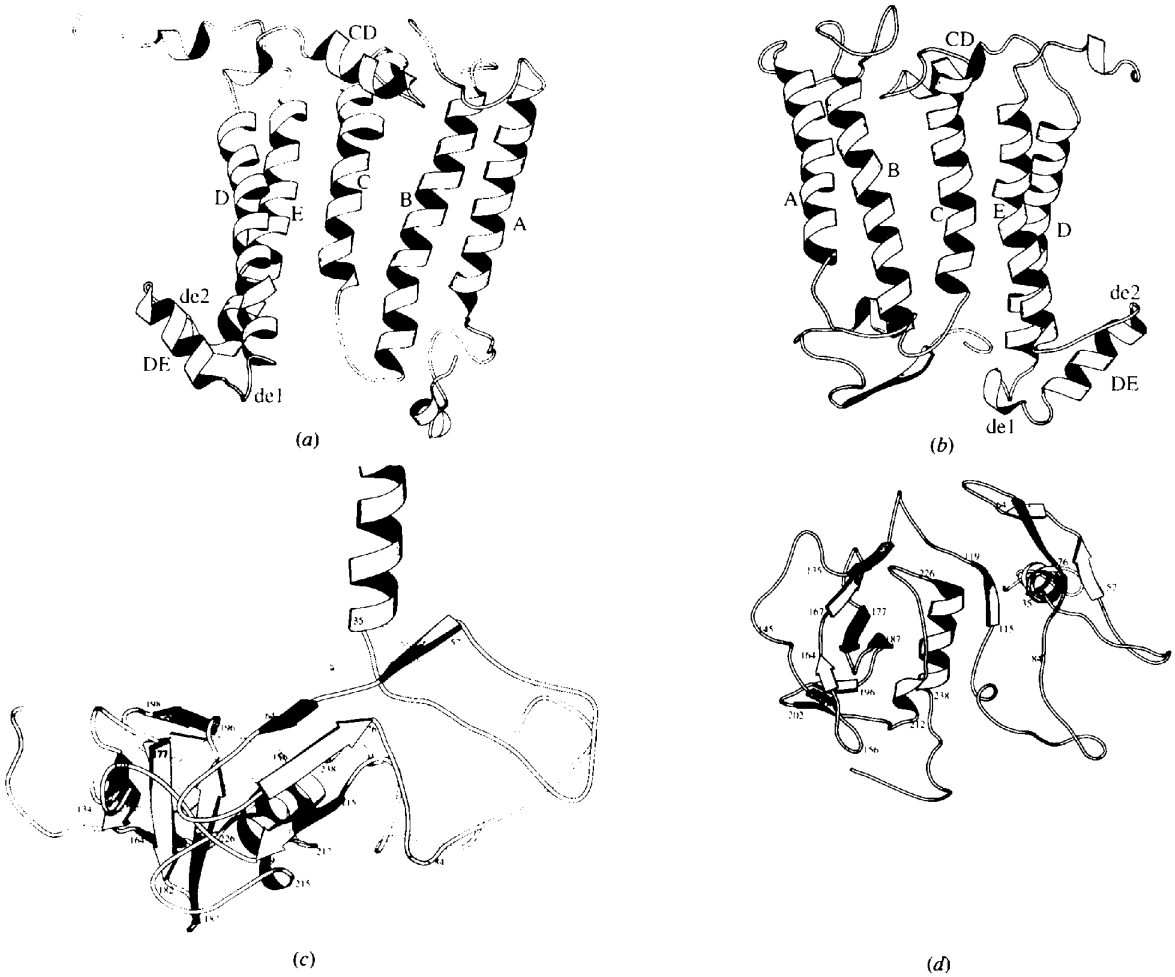

Fig. 4. Schematic drawings of the isolated subunits, with labelling of the secondary-structure elements. (*a*) *L* subunit; (*b*) *M*; (*c*) and (*d*) *H*. In (*c*) the scale is enlarged, the N terminus and part of the transmembrane helix of *H* are not shown. The orientation in (*a*), (*b*), and (*c*) is the same as in Fig. 1(*a*); in (*d*) *H* is viewed in another orientation, with the transmembrane helix axis perpendicular to the figure plane.

diversely oriented with respect to the symmetry axis. *D* helices show a pronounced curvature leaving space for the bulky Bchl's dimer (Fig. 1*a*).

The connections between these helices contain several short helices (Table 2) and depart from the local twofold symmetry (see Figs. 4*a* and 4*b*). It is worth noting that the connecting sequence between the *D* and *E* helices (named *de*) is different in *M* and *L*; in both subunits it contains a short helix (*DE*) flanked by two loop regions (de_1 and de_2) and the de_2 loop is longer in *M* than in *L*. The N-terminal region, before helix *A*, is also longer in *M*. In contrast, the connection between the *A* and *B* helices is longer in *L*.

The *H* chain (Figs. 4*c* and 4*d*) is the only subunit containing β-sheets. Its short N-terminal region (*H*1–*H*12) located on the periplasmic surface is followed by the only transmembrane helix (*H*12–*H*35). Residues *H*52 to *H*115, starting with three β-strands, are formed of large loops extended along the surface of the *L*–*M* complex in intimate contact with it. The rest of the *H* chain is intricately folded into a globular domain, which contains a system of antiparallel β-sheets between residues *H*153 and *H*205. Before the C terminus, an α-helix (residues *H*228 to *H*239) is observed, whose axis is almost perpendicular to the pseudo-twofold axis.

In this structure most polar and charged residues are segregated into the periplasmic connections, the

Table 2. *α-Helices of L and M: localization and definition (residue range and length)*

θ, angle between the pseudo-twofold symmetry axis and the mean axis of each hydrophobic helix.

		L	*M*	θ (°)
Transmembrane	*A*	33–53 (21)	55–76 (22)	25
	B	83–110 (28)	114–138 (25)	16
	C	116–138 (23)	145–167 (23)	8
	D	172–198 (27)	200–226 (27)	33
	E	225–253 (29)	263–286 (24)	19
Periplasmic	*CD*	151–163 (13)	181–188 (8)	
	—	—	244–255 (12)	
Cytoplasmic	—	—	37–42 (6)	
	DE	209–220 (12)	244–255 (12)	

Spheroidene $C_{41}H_{60}O$

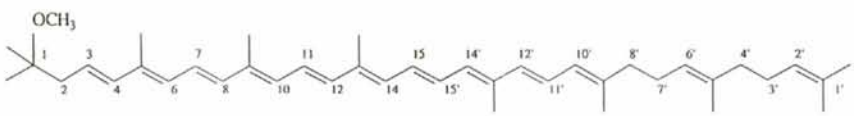

1,2-Dihydroneurosporene $C_{49}H_{60}$

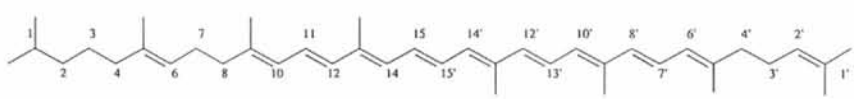

Fig. 5. Chemical formula of spheroidene and of 2,4 dihydroneurosporene (carotenoids bound to *Rb. sphaeroides* Y and *Rps. viridis* RC's, respectively).

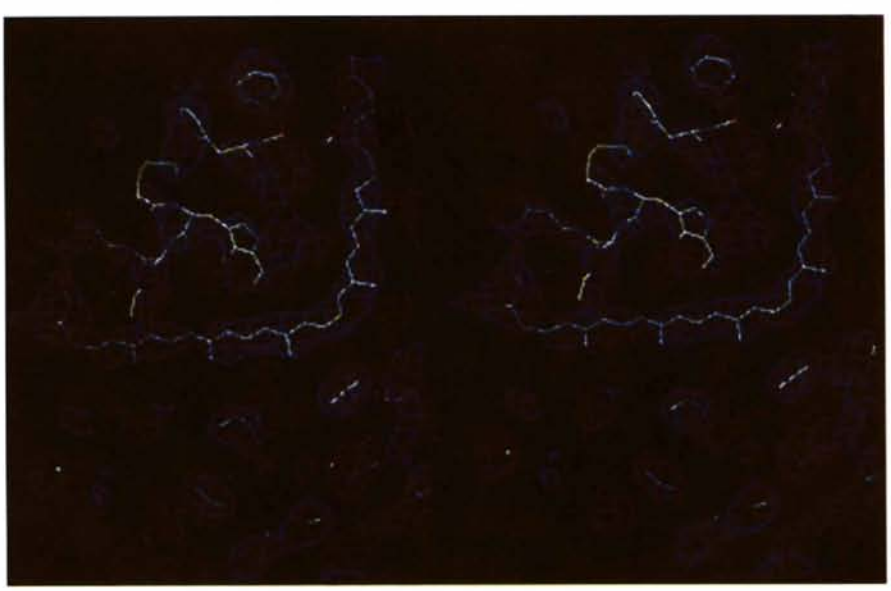

Fig. 6. Stereoview of the $2F_o - F_c$ electron-density map for the spheroidene molecule.

cytoplasmic ends of the transmembrane helices and in *H*. A high proportion of *L* and *M* Trp residues (22 out of 36) are observed in a layer beneath the periplasmic surface with most of their cyclic atoms perpendicular to this surface facing towards the pigments.

Carotenoid

RC from the Y strain of *Rb. sphaeroides* contains a carotenoid molecule which is a spheroidene (Fig. 5). This long polyenic chain adopts a *cis* conformation, predicted to be 15-15′ by Raman spectroscopy (Lutz, Szponarski, Berger, Robert & Neumann, 1987). The initial Fourier difference map showed positive density at close proximity from monomeric BC_{MA}. It was possible to build a spheroidene molecule in this density with a *cis* conformation (Arnoux *et al.*, 1989). In the refined map, the electron density extends to both ends of the molecule and allows to discriminate without ambiguity the terminal *sp*3 and *sp*2 C atoms (Fig. 6). Both extremities of the chain are surrounded by bulky hydrophobic residues of the *M* subunit: Phe67, Phe68, Phe85 and Trp75 around C1, Phe123 and Phe162 around C1′. The carotenoid conformation deviates from planarity in its non-conjugated part (C1′–C8′ region). At the level of the central *cis* bond the closest distance (2.9 Å) is observed between C15′ C atom of spheroidene and acetyl O atom of BC_{MA} ring I.

Manganese-binding site

The Mn^{2+} ion, which is located on the local twofold symmetry axis, is sixfold coordinated (Table 3). Glutamic acid (*M*234) provides two equidistant ligands. The other four ligands are symmetry-related histidines from *L* and *M* (*L*190, *L*230, *M*210, *M*266). Thus, the Mn^{2+}-binding site is similar to that of Fe^{2+} in other RC's (Michel, Epp & Deisenhofer, 1986; Allen, Feher, Yeates, Komiya & Rees, 1988).

Hydrogen bonds and salt bridges

Besides the hydrogen bonds formed in the backbone of α-helices or β-sheets, a number of hydrogen bonds are observed which contribute to the stability of the individual subunits, to their mutual interactions and to the binding of pigments.

Within each subunit, hydrogen bonds occuring between the main-chain and side-chain residues were analyzed. There are 35, 40 and 24 such bonds within the *L*, *M* and *H* subunits, respectively, with an average distance of 3.0 Å.

Hydrogen bonds between side chains of two residues in the same subunit are also observed (Table 4). There are six, 12 and 20 such interactions within *L*, *M* and *H*, respectively, with an average length of 2.9 Å; they include several salt bridges. For *L* and *M*, these bonds are located either on the periplasmic or cytoplasmic sides. Obviously, the largest number of such interactions, including 12 salt bridges, occurs in *H*, which is the most hydrophilic subunit.

Finally, subunits are tightened by interchain hydrogen bonds and salt bridges, listed in Table 5.

Between *L* and *M* these bonds principally occur on the hydrophilic cytoplasmic interface. There, the *de* loops and *DE* helix of one subunit are bridged with the end of *B* helix of the other one. The cytoplasmic extremities of E_L and D_M are also bridged, and the N terminus of *M* interacts in this region.

Table 3. *Distances* (Å) *between the metal ion and its six ligands in the metal-binding site*

Metal ion: Mn^{2+} in Y strain and Fe^{2+} in R26 RC and *Rps. viridis* RC.

	Y	R26*	*Rps. viridis*†
His*L*190 NE2	2.1	2.1	2.0
His*L*230 NE2	2.1	2.2	2.4
His*M*219 NE2	2.0	2.2	2.1
His*M*266 NE2	2.0	2.1	2.0
Glu*M*234 OE1	2.1	2.2	2.2
Glu*M*234 OE2	2.1	2.2	2.0

* Data from PDB entry 4RCR.
† Data from PDB entry 1PRC.

Table 4. *Hydrogen bonds, salt bridges* (*) *and related distances* (*d*) *between side chains of the same subunit*

Residue		Residue		*d*(Å)
Glu *L*6	OE1	Arg*L*10	NE	3.2
Glu *L*6	OE1	Arg*L*10	NH1	3.2*
Thr *L*90	OG1	Tyr*L*148	OH	2.8
Asp*L*155	OD2	Asn*L*159	ND2	3.2
Asn*L*166	OD1	His*L*168	ND1	2.4
Glu *L*205	OE1	Arg*L*207	NH1	3.5*
Asp*L*213	OD2	Ser*L*223	OG	2.4
Asn*M*25	ND2	Asn*M*28	OD1	3.0
Ser *M*93	OG	Glu*M*95	OE1	2.9
Glu *M*95	OE1	Ser*M*181	OG	3.3
Glu *M*95	OE2	Ser*M*181	OG	3.0
Tyr *M*101	OH	Glu*M*111	OE1	3.0
Tyr *M*101	OH	Glu*M*111	OE2	3.1
Ser *M*119	OG	Tyr*M*177	OH	2.7
Glu *M*234	OE2	His*M*266	NE2	2.6
Arg *M*241	NE	Glu*M*246	OE1	2.7
Arg *M*241	NE	Glu*M*246	OE2	2.8
Arg *M*241	NH2	Glu*M*246	OE1	2.9*
Tyr *M*295	OH	Gln*M*299	OE1	3.4
Thr *H*5	OG1	Asp*H*11	OD2	2.9
Asp*H*11	OD1	Ser*H*14	OG	2.7
Glu *H*34	OE2	Arg*H*37	NE	3.2*
Glu *H*34	OE2	Arg*H*37	NH1	3.0*
Arg *H*89	NH1	Glu*H*94	OE2	3.1*
Arg *H*117	NH1	Asp*H*231	OD2	3.2*
Arg *H*117	NH1	Asp*H*231	OD1	2.6*
Asn*H*129	ND2	Glu*H*224	OE1	3.4
Lys *H*130	NZ	Glu*H*173	OE1	3.0
Lys *H*130	NZ	Asp*H*170	OD1	2.6*
Lys *H*130	NZ	Asp*H*170	OD2	2.8*
Asp*H*157	OD1	Ser*H*210	OG	2.4
Asp*H*157	OD2	Ser*H*210	OG	3.1
Lys *H*163	NZ	Glu*H*182	OE2	2.5*
Asp*H*170	OD1	Arg*H*177	NH1	2.8*
Glu *H*173	OE2	Arg*H*177	NH1	2.8*
Glu *H*180	OE1	Thr*H*188	OG1	2.9
Asp*H*185	OD2	Ser*H*187	OG	3.3
Lys *H*247	NZ	Glu*H*258	OE2	2.7*

Table 5. *Hydrogen bonds and salt bridges* (*) *between different subunits and related distances* (*d*)

Residue		Residue		*d* (Å)
Arg *L*103	NH2	Thr *M*255	O	2.8
Leu *L*111	O	Arg *M*247	NH1	2.6
Gly *L*112	O	Arg *M*247	NH2	3.3
Tyr *L*115	O	Gln *M*4	NE2	3.3
His *L*116	NE2	Gln *M*4	OE1	3.1
Thr *L*152	N	Pro *M*305	OT2	3.1
Asn *L*166	ND2	Asn *M*187	OD1	3.0
His *L*168	ND1	Leu *M*183	O	3.0
Asn *L*183	OD1	Ala *M*213	N	2.8
His *L*190	NE2	Glu *M*234	OE1	2.9
Ser *L*196	O	Gly *M*143	N	3.2
Glu *L*201	OE1	Lys *M*144	NZ	3.4*
Arg *L*207	NH2	Met *M*140	O	2.6
Arg *L*207	NH2	Glu *M*22	OE1	3.0*
Leu *L*219	O	Arg *M*132	NH1	2.8
Tyr *L*222	OH	Asn *M*44	O	3.3
Ser *L*223	O	Asn *M*44	ND2	3.4
Thr *L*226	OG1	Glu *M*232	O	3.4
His *L*230	NE2	Glu *M*234	OE1	2.7
Arg *L*231	NH1	Ile *M*6	O	2.7
Arg *L*231	NH1	Phe *M*42	O	2.7
Arg *L*231	NH2	Asn *M*5	OD1	2.9
Gly *L*233	O	Ala *M*217	N	3.4
Ser *L*237	OG	Ala *M*213	O	3.3
Trp *L*266	NE1	Arg *M*87	O	2.6
Ser *L*4	OG	Gly *H*39	O	2.8
Lys *L*8	NZ	Glu *H*81	OE2	2.9*
Arg *L*10	O	His *H*98	N	3.2
Trp *L*25	N	Gly *H*95	O	2.6
Met *L*206	N	Ile *H*65	O	3.4
Asp *L*210	O	Gly *H*125	N	3.4
Arg *M*13	O	His *H*141	N	2.8
Gly *M*14	N	Gln *H*174	OE1	3.1
Ser *M*227	O	Gln *H*194	NE2	3.5
Glu *M*232	OE1	Arg *H*177	NH2	2.7*
Arg *M*233	NH1	Glu *H*230	OE1	2.8*
Arg *M*233	NH2	Glu *H*230	OE2	3.0*
Glu *M*236	OE1	Leu *H*123	N	3.2
Glu *M*236	OE2	Arg *H*118	NH2	2.9*
Asp *M*240	O	Arg *H*117	NE	2.6
Asp *M*240	OD2	Arg *H*118	NH1	3.4*
Arg *M*241	NH1	Glu *H*79	OE1	2.9*
Arg *M*241	NH1	Glu *H*38	OE2	2.8*
Thr *M*243	OG1	Ser *H*113	O	3.3
Trp *M*297	NE1	Asp *H*11	OD1	3.0
His *M*301	NE2	Asn *H*9	O	3.5

Between *L* and *H* a few bonds are observed on the cytoplasmic side and concern principally backbone interactions. Four out of six are located in the N-terminus region of *L*.

Between *M* and *H* all the bonds are located on the cytoplasmic part of the RC, except for a few which occur on the periplasmic surface, between the C terminus of *M* and N terminus of *H*. Most of the interchain salt bridges are formed between these subunits: a series of charged residues in *M* (from *M*232 to *M*241) in the de_1 loop interact with *H* residues (*H*117–*H*118, *H*230, *etc.*). A few hydrogen bonds link otherwise the N terminus of *M* and *H* in the interface region between *H* and *LM*.

At the level of the pigments and cofactors which are buried within *L* and *M*, carbonyl groups of several pigments are hydrogen bonded to neighbouring residues (Arnoux, Ducruix & Reiss-Husson, 1995).

Interactions between subunits.

The overall accessible area of the complex, 39 120 Å^2, is equally balanced between the three subunits *L*, *M* and *H*, which contribute 12 070, 12 930 and 14 120 Å^2, respectively. The buried surface area between *L* and *M* is 4400 Å^2, a value similar to the buried surface area between *LM* and *H* (4150 Å^2). More extensive contacts of *H* with *M* than with *L* are reflected in the values of the buried surface area, 2700 Å^2 between *H* and *M*, and 1550 Å^2 between *H* and *L*.

Interactions between L and M. Accessible area of individual residues in the *LM* complex may be compared with that calculated for the isolated *L* or *M* subunit. A plot of the differences is shown in Figs. 7(*a*) and 7(*b*). A roughly similar pattern is observed for the distribution of interacting residues along *L* and *M* sequences. Namely, in *L* and *M* all transmembrane helices except *A* and also the *BC* and *DE* connections are more or less involved in intersubunit contacts.

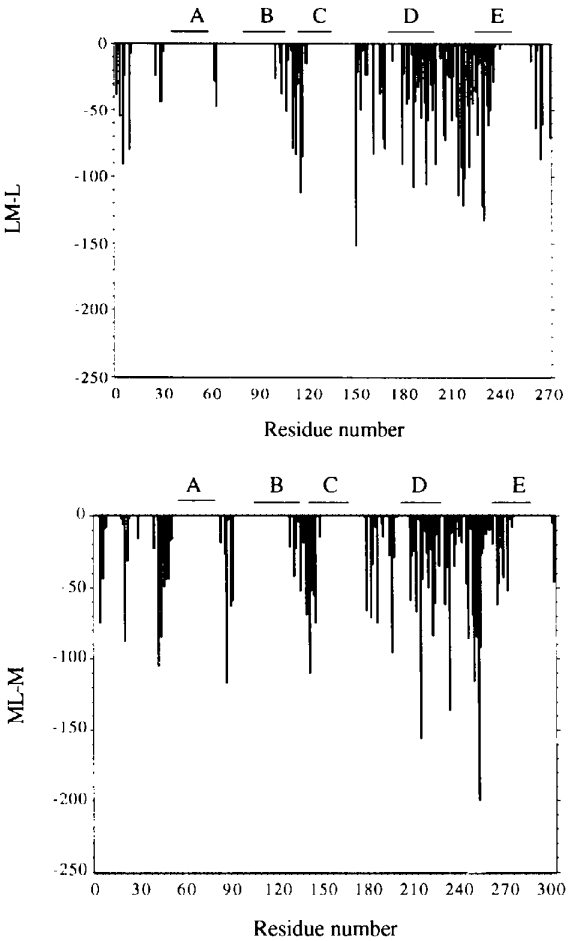

Fig. 7. Differences (Å^2) between the accessible area of individual residues in the *LM* complex and (*a*) in the isolated *L* subunit (*b*) in the isolated *M* subunit.

When neighbouring residues in contact are analyzed in more detail, the pseudo-twofold symmetry between L and M also applies to contacts in several regions: $B_L \leftrightarrow DE_M$ related to $B_M \leftrightarrow DE_L$ and $D_L \leftrightarrow (D_M+C_M)$ related to $D_M \leftrightarrow (D_L + C_L)$. However, this symmetry does not apply for the cytoplasmic end of the C helices: $C_L \leftrightarrow \text{Nterm}M$, $C_M \leftrightarrow (DE_L + D_L)$.

Interactions between L, M and H. In several regions of the RC, residues from the H chain, scattered throughout this subunit, are in close contact with both L and M (Fig. 8). Hydrophobic interactions occur between the E_M helix and both D_L and H transmembrane helices. The other interacting regions involve mainly the surroundings of the N-terminus of L and M, the *bc* loop of L, and the *de* connection of L and M.

(i) *N-terminus region of the L chain.* 17 out of the first 28 residues of L are in close contact with either the M-chain residues (7) or H-chain residues (9) through van der Waals interactions, hydrogen bonds and one salt bridge (*cf.* Table 5). The N-terminus region of L is thus embedded between the DE_M helix, the cytoplasmic end of transmembrane helix of H and residues H81, H87 and H95–H98.

(ii) *N-terminus region of the M chain.* The extended N-terminus region of M lies along the H-chain buried surface (H138–H146, H169, H174–H176, H193–H196, H206 and H241). The 15 first residues of M are otherwise in close contact with the cytoplasmic end of C_L helix.

(iii) *The de_1 loop of L.* This loop (L201–L207) is connected to M by a salt bridge and to H by one main-chain···main-chain hydrogen bond. There are also several van der Waals contacts with M (M140, M144 and M235) and with H (H65–H67).

(iv) *H108 to H125 region.* This region of H is the longest one interacting with L and M. Hydrophobic interactions prevail around residues H108–H112 (GVGPA) surrounded by other apolar segments: L11–L14 (VPGG), L111–L114 (LGIG), H84–H88 (PIALA), H237–H241 (VAGGL). In this region three proline residues H100, H104, L12 are at less than 10 Å from Pro$H$111. Electrostatic interactions take place from H113 to H125 with the DE_L helix and with the de_1 loop of M (Fig. 9).

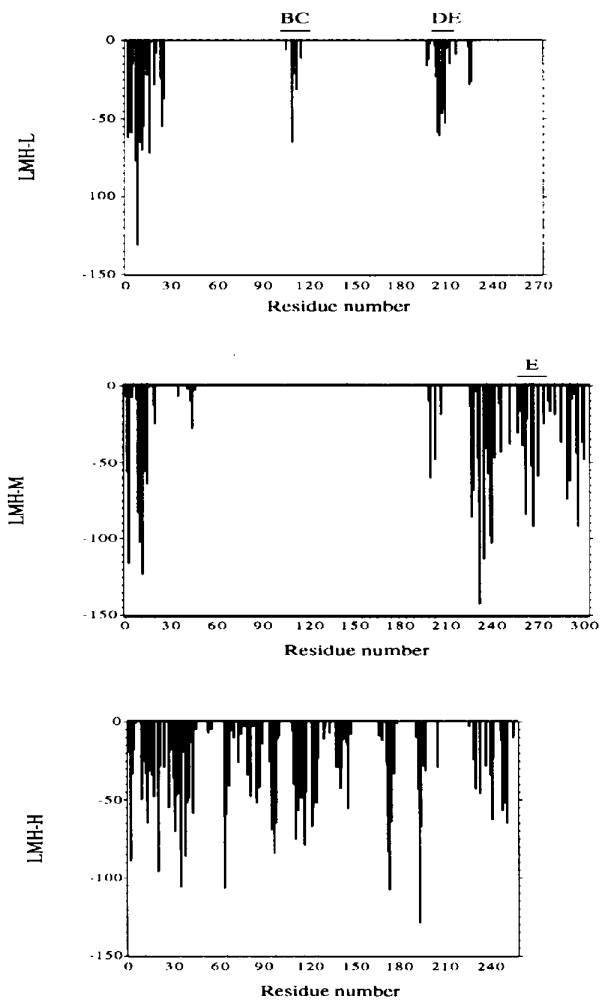

Fig. 8. Differences (Å^2) between the accessible area of individual residues in the *LMH* complex and (*a*) in isolated L subunit (*b*) in the isolated M subunit (*c*) in the isolated H subunit.

Crystal packing

Crystal-packing contacts mainly concern the cytoplasmic H138–H166 surface of H and the periplasmic surface of L and M. They involve the connection between A_L and B_L, and the C terminus of M. Residues H138–H141 are in close contact with L66–L67 and H138–H150 with M292–M305 (Fig. 10). Residues H150 and H163 are also in contact with the first two residues of H belonging to another symmetry-related RC molecule. No salt bridges are observed but both hydrogen bonds and hydrophobic interactions occur.

It should be stressed that in this membrane protein crystal, detergent associated with the RC occupies about one third of the cell volume (Roth, Arnoux, Ducruix & Reiss-Husson, 1991). β-D-octylglucoside is mainly organized in a belt around the hydrophobic part of the transmembrane helices. These belts are interconnected into ribbons running along the *b* axis. The paucity of protein contacts along this direction and the possible flexibility of the detergent ribbons could explain the anisotropy of the crystalline order. Morever, polar contacts are established between the protein at residues Asp$H$46, Asp$H$83, Arg$H$85, Lys$H$106, Asp$H$107 and the hydrophilic surface of the detergent phase associated with a neighbouring RC.

Discussion

The study of the three-dimensional structure of the RC from *Rb. sphaeroides* Y has provided new results about

two specific features which are still largely debated: the conformation of the carotenoid molecule and the specificity and functional role of the bound metal ion (here manganese).

The unique carotenoid molecule which is part of the RC in all wild-type strains of purple bacteria confers protection against photo-oxidation damage, a biologically important function which is clearly related to the particular structure of this pigment. Quite early on (Lutz, Kleo & Reiss-Husson, 1976) it was shown that this carotenoid has a special *cis* conformation, different from the all-trans one which is the most stable *in vitro* and which prevails in the antenna complexes of these bacteria. Crystallographic analysis of RC's from *Rps. viridis* (Deisenhofer & Michel, 1989) and from *Rb. sphaeroides* wild-type strains Y (Arnoux *et al.*, 1989) and 241 (Yeates *et al.*, 1988) were in agreement for the localization of the *cis* bond, in close proximity to ring I of BC_{MA}. However, ambiguities persisted for the precise stereochemistry of the molecule: the position of the *cis* bond, the existence and position of additional twists. In *Rps. viridis*, the carotenoid (which is 2,4-dihydroneurosporene, see Fig. 5) has been fitted in the electron density as a 13′-14′-*cis* isomer. However the density does not extend to both ends of the molecule: it is missing for C atoms 1 to 3 and 1′ to 7′ as mentioned in the PDB entry (1PRC). Similarly, before the refinement of *Rb. sphaeroides* Y structure (Arnoux *et al.*, 1989) only the central part of spheroidene could be fitted in the density. It was built as a central 15-15′-*cis* isomer on the basis of Raman spectroscopy; the positions of both ends of the molecule were dictated by the shape of the cavity delimited by neighbouring residues. These uncertainties and conflicting results did not provide a convincing and unique model, as pointed out in a recent review (Frank, 1993). However, after refinement of the Y RC structure, our previous model is confirmed and supported by more complete data. Indeed the electron density extends now to the whole carotenoid molecule (Fig. 6); the *B* values for individual spheroidene C atoms are in a satisfactory

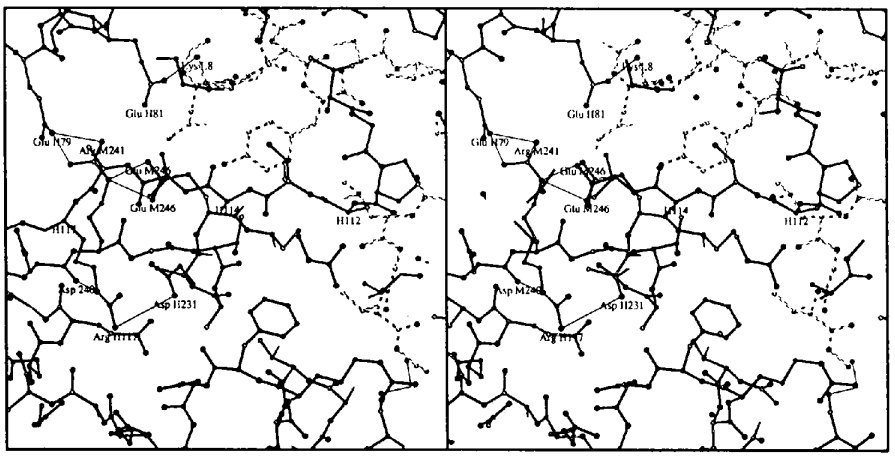

Fig. 9. Stereoview of the *H*108–*H*125 region drawn as a ball-and-stick diagram. *L* subunit is drawn as a broken line, *M* as an open line and *H* as a shaded line.

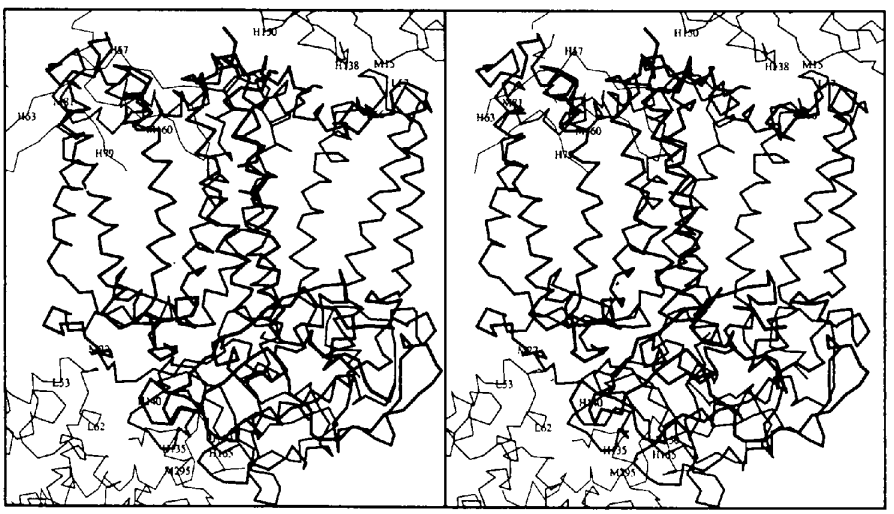

Fig. 10. Packing contacts. The protein (in bold) is represented as a C_α trace, closest neighbours are indicated in thin lines.

range (between 13.5 and 54.1 Å^2) as compared to the mean B value (34.7 Å^2). Discrimination between C1 and C1′ atoms is reliable because the bulky methoxy group in C1 is well defined in the density. Thus, the best fit for spheroidene in the electron density is a central 15-15′-*cis* isomer, with a planar conformation from C2 to C8′, and additional out-of-plane twists at the C7′ and C4′ atoms. We would like to stress that there is no crystallographic support for fitting with a non-central isomer such as a 13–14-*cis*. Moreover a general consensus for a central *cis* conformation of spheroidene has been reached, from convincing resonance Raman data (Koyama, Takii, Saiki & Tsukida, 1983; Lutz, Szponarski, Berger, Robert & Neumann, 1987) and recent NMR experiments (De Groot *et al.*, 1992).

Another distinctive feature of Y RC is the presence of manganese as the metal ion interacting with the quinones (Rutherford, Agalidis & Reiss-Husson, 1985), instead of iron which is present in RC's of *Rps. viridis* and in other *Rb. sphaeroides* strains. The characteristics of the Mn^{2+}-binding site are shown here to be identical to those of Fe^{2+} in the other RC's: the ligands and their positions are the same (Table 3). It has been shown that in the Y strain, Mn^{2+} may be replaced in the RC by other metals by modifying their relative abundance during growth of the bacteria. Fe^{2+} (Rutherford, Agalidis & Reiss-Husson, 1985), as well as Zn^{2+}, could thus be substituted (Feezel *et al.*, 1990), while the stability of the isolated RC's would not be impaired. These exchanges probably occur without any structural modification, as the protein structure seems to be stable enough to tolerate a number of divalent metal ions. *In vitro* replacement of Fe by other metals in *Rb. sphaeroides* R26 RC's has also be achieved without alteration of electron transport (Debus, Feher & Okamura, 1986).

The present work shows that the three-dimensional structure of wild-type *Rb. sphaeroides* RC is highly homologous to those of the R26 strain (Allen, Feher, Yeates, Komiya & Rees, 1988; Chang, El-Kabbani, Tiede, Norris & Schiffer, 1991) and of *Rps. viridis* (Deisenhofer & Michel, 1989). For a detailed comparison of Y and R26 structures, we used the refined coordinates published recently by Yeates *et al.* (1988) (PDB entry 4RCR), for which completeness of X-ray data is close to our set. The best fit between the Cα atoms of the 11 transmembrane helices of the two structures indicates an r.m.s. deviation of 0.87 Å. This r.m.s. value is 1.0 when the comparison is made between Y and *Rps. viridis* RC's. In these bacterial species the backbones of the transmembrane helices are thus very similar, despite the rather low conservation of hydrophobic residues exposed to the membrane (Rees, Komiya, Yeates, Allen & Feher, 1989). The only significant difference concerns the transmembrane helix of *H* because of the insertion of one residue (Trp*H*21) in *Rps. viridis*, amidst the helix (Michel, Weyer, Gruenberg & Lottspeich, 1985), which results in a slightly distorted geometry between *H*29 and *H*31.

Superposition of the transmembrane helices of the three structures also gives a very good fit for the exposed connections between helices on the periplasmic surface. This was less expected, because in the *Rps. viridis* crystal this region is bound to and shielded by the tetrahaemic cytochrome whereas in the *Rb. sphaeroides* crystal it is exposed to the solvent. In spite of the same folding, there are several inversions of charged structurally homologous residues in the *L* connections. For example, in the AB_L connection, *L*72 and *L*82 are Lys and Glu in *Rps. viridis*, and Glu and Lys in *Rb. sphaeroides*, respectively; in the C-terminal region, *L*257 and *L*268 are Arg and Asp in the former, Asp and Lys in the latter.

For the cytoplasmic part of the RC and particularly for *H*, the fit between *Rps. viridis* and both *Rb. sphaeroides* structures is less reliable while the secondary structure is conserved. The low sequence conservation of the *H* subunit (Williams, Steiner & Feher, 1986) does not lead to different foldings. The amino-acid composition of *H* indicates a higher abundance of proline residues in *Rb. sphaeroides* (8.8%) than the average value (5.1%) given for soluble proteins (McCaldon & Argos, 1988). 13 proline residues out of the 23 in the *Rb. sphaeroides H* subunit are conserved in the three other bacterial species for which the *H* sequence is known (Berard & Gingras, 1991); some of these are located in structural elements such as the polar domain following the transmembrane helix and in β-strands. But because of the limited number of sequences of RC's, it seems rather hazardous to draw conclusions on the role of prolines in these complexes.

Evidence for the regions of interaction between subunits described above for Y RC may also be provided by the same methods for *Rps. viridis* RC and appear to be largely conserved. In these interactions, which evidently contribute to the overall packing energy of the complex, one should not underestimate the role of the *H* subunit. This subunit is sometimes not considered to be essential for the RC function because it does not interact directly with the pigments and cofactors. Yet interactions between *H*, *L* and *M*, particularly in the *de* loops, contribute to the conformation and the geometry of the quinones and metal-binding sites. This could explain why a loss of the metal may occur when *H* is split off from the RC *in vitro* (Agalidis, Nuijs & Reiss-Husson, 1987).*

The authors are grateful to Drs Chantal Astier and Martine Picaud for cloning and sequencing the RC

* Atomic coordinates have been deposited with the Protein Data Bank, Brookhaven National Laboratory (Reference: 1YST). Free copies may be obtained through The Managing Editor, International Union of Crystallography, 5 Abbey Square, Chester CH1 2HU, England (Reference: GR0395).

genes, to Drs Ileana Agalidis and Pierre Sebban for helpful discussions, and to Drs Chong Hwan Chang and Marianne Schiffer for their advice and assistance during the early phase of structure determination. The authors thank the staff of LURE (Orsay) for making station D43 of LURE available to them. This work was supported by a grant from the Ministère de la Recherche et de la Technologie, décision 86.C.0684.

Note added in proof: refined structures from the RC's from two other *Rb. sphaeroides* strains were recently published (Chino *et al.*, 1994; Ermler, Fritzsch, Buchanan & Michel, 1994).

References

AGALIDIS, I. NUIJS, A. M. & REISS-HUSSON, F. (1987). *Biochim. Biophys. Acta*, **890**, 242–250.

ALLEN, J. P., FEHER, G., YEATES, T. O., KOMIYA, H. & REES, D. C. (1988). *Proc. Natl Acad. Sci. USA*, **85**, 8487–8491.

ARNOUX, B., DUCRUIX, A., ASTIER, C., PICAUD, M., ROTH, M. & REISS-HUSSON, F. (1990). *Biochimie*, **72**, 525–530.

ARNOUX, B., DUCRUIX, A. & REISS-HUSSON, F. (1995). In preparation.

ARNOUX, B., DUCRUIX, A., REISS-HUSSON, F., LUTZ, M., NORRIS, J., SCHIFFER, M. & CHANG, C. H. (1989). *FEBS Lett.* **58**, 47–50.

BERARD, J. & GINGRAS, G. (1991). *Biochem. Cell Biol.* **69**, 122–131.

BRÜNGER, A. T., KURIYAN, J. & KARPLUS, M. (1987). *Science*, **235**, 458–460.

BRZOZOWSKI, A. M., DEREWENDA, Z. S., DODSON, E. J., DODSON, G. G. & TURKENBURG, J. P. (1992). *Acta Cryst.* A**32**, 307–319.

BUCHANAN, S. K., FRITZSCH, G., ERMLER, U. & MICHEL, M. (1993). *J. Mol. Biol.* **230**, 1311–1314.

CHANG, C. H., EL-KABBANI, O., TIEDE, D., NORRIS, J. & SCHIFFER, M. (1991). *Biochemistry*, **30**, 5352–5360.

CHANG, C. H., TIEDE, D., TANG, J., SMITH, U., NORRIS, J. & SCHIFFER, M. (1986). *FEBS Lett.* **205**, 82–86.

COGDELL, R. J. & FRANK, H.A. (1987). *Biochim. Biophys. Acta*, **895**, 63–79.

COLLABORATIVE COMPUTATIONAL PROJECT, NUMBER 4 (1994). *Acta Cryst.* D**50**, 760–763.

COLLOC'H, N., ETCHEBEST, C., THOREAU, E., HENRISSAT, B. & MORNON, J. P. (1993). *Protein Eng.* **6**, 377–382.

DEBUS, R. J., FEHER, G. & OKAMURA, M. Y. (1986). *Biochemistry*, **25**, 2276–2287.

DE GROOT, H. J. M., GEBHARD, R., VAN DER HOEF, K., HOFF, A. J., LUGTENBURG, J., VIOLETTE, C. A. & FRANK, H. A. (1992). *Biochemistry*, **31**, 12446–12450.

DEISENHOFER, J., EPP, O., MIKI, K., HUBER, R. & MICHEL, H. (1985*a*). *J. Mol. Biol.* **180**, 395–398.

DEISENHOFER, J., EPP, O., MIKI, K., HUBER, R. & MICHEL, H. (1985*b*). *Nature (London)*, **318**, 618–624.

DEISENHOFER, J. & MICHEL, H. (1989). *EMBO J.* **8**, 2149–2170.

DUCRUIX, A., ARNOUX, B. & REISS-HUSSON, F. (1988). *The Photosynthetic Reaction Center: Structure and Dynamics*, Vol. 149, edited by J. BRETON & A. VERMEGLIO, pp. 21–25. New York: Plenum Press.

DUCRUIX, A. & REISS-HUSSON, F. (1987). *J. Mol. Biol.* **193**, 419–421.

EL-KABBANI, O., CHANG, C. H., TIEDE, D., NORRIS, J. & SCHIFFER, M. (1991). *Biochemistry*, **30**, 5361–5369.

ENGH, R. H. A. & HUBER, R. (1991). *Acta Cryst.* A**47**, 392–400.

FEEZEL, L. L., REISS-HUSSON, F., AGALIDIS, I., SMITH, U. H., THURNAUER, M. C. & NORRIS, J. (1990). *Appl. Magn. Res.* **1**, 255–265.

FRANK, H. (1993). *The Photosynthetic Reaction Center*, Vol. 2, edited by J. DEISENHOFER & J. R. NORRIS, pp. 221–237. New York: Academic Press.

FOLOPPE, N., FERRAND, M., BRETON, J. & SMITH, J. C. (1995). In preparation.

JONES, T. A. (1978). *J. Appl. Cryst.* **11**, 268–272.

KABSCH, W. & SANDER, C. (1983). *Biopolymers*, **22**, 2577–2637.

KOMIYA, H., YEATES, T. O., REES, D. C., ALLEN, J. P. & FEHER, G. (1988). *Proc. Natl Acad. Sci. USA*, **85**, 9012–9016.

KOYAMA, Y., TAKII, T., SAIKI, K. & TSUKIDA, K. (1983). *Photobiochem. Photobiophys.* **5**, 139–150.

KRAULIS, P. J. (1991). *J. Appl. Cryst.* **24**, 946–950.

LEE, B. K. & RICHARDS, F. M. (1971). *J. Mol. Biol.* **55**, 379–400.

LUTZ, M., KLEO, J. & REISS-HUSSON, F. (1976). *Biochem. Biophys. Res. Commun.* **69**, 711–717.

LUTZ, M., SZPONARSKI, W., BERGER, G., ROBERT, B. & NEUMANN, J. M. (1987). *Biochim. Biophys. Acta*, **894**, 423–433.

LUZZATI, P. V. (1952). *Acta Cryst.* **5**, 802–810.

MCCALDON, P. & ARGOS, P. (1988). *Proteins*, **4**, 99–122.

MICHEL, H., EPP, O. & DEISENHOFER, J. (1986). *EMBO J.* **5**, 2445–2451.

MICHEL, H., WEYER, K. A., GRUENBERG, H. & LOTTSPEICH, F. (1985). *EMBO J.* **4**, 1667–1672.

OTWINOWSKI, Z. (1993). *Proceedings of CCP4 Study Weekend*, edited by L. SAWYER, N. ISAACS & S. BAILEY, pp. 56–62. Warrington, England: SERC Daresbury Laboratory.

RAY, W. J. & PUVATHINGAL, J. (1985). *Anal. Biochem.* **146**, 307–312.

REES, D. C., KOMIYA, H., YEATES, T. O., ALLEN, J. P. & FEHER, G. (1989). *Annu. Rev. Biochem.* **58**, 607–633.

REISS-HUSSON, F. & MÄNTELE, W. (1988). *FEBS Lett.* **239**, 78–82.

RICHARDS, F. M. & KUNDROT, C. E. (1988). *Proteins*, **3**, 71–84.

ROTH, M., ARNOUX, B., DUCRUIX, A. & REISS-HUSSON, F. (1991). *Biochemistry*, **30**, 9403–9413.

RUTHERFORD, A. W., AGALIDIS, I. & REISS-HUSSON, F. (1985). *FEBS Lett.* **182**, 151–157.

SKLENAR, H., ETCHEBEST, C. & LAVERY, R. (1989). *Proteins*, **6**, 46–60.

WILLIAMS, J. C., STEINER, J. A. & FEHER, G. (1986). *Proteins*, **1**, 312–325.

YEATES, T. O., KOMIYA, H., CHIRINO, A., REES, D., ALLEN, J. P. & FEHER, G. (1988). *Proc. Natl Acad. Sci. USA*, **85**, 7993–7997.